DIRECT NUMERICAL SIMULATION OF A TURBULENT CHANNEL FLOW ACROSS A SUDDEN EXPANSION: EFFECTS OF SPANWISE ROTATION

Eric Lamballais

Institute PPRIME

Department of Fluid Flow, Heat Transfer and Combustion

Université de Poitiers, CNRS, ENSMA

Téléport 2 - Bd. Marie et Pierre Curie B.P. 30179

86962 Futuroscope Chasseneuil Cedex, France

eric.lamballais@univ-poitiers.fr

Marcel Lesieur

Laboratoire des Ecoulements Géophysiques et Industriels

Académie des sciences

Grenoble-INP, UJF, CNRS

BP 53, F-38041 Grenoble cedex 9, France

marcel.lesieur@hmg.inpg.fr

ABSTRACT

The effects of a spanwise rotation on the channel flow across a sudden expansion are investigated using DNS. Four rotation regimes are considered with the same Reynolds number $Re = 5000$ and ratio expansion $Er = 1.5$. Upstream from the expansion, inflow turbulent conditions are generated realistically for each rotation rate through a very simple and efficient technique of recycling without the need of any precursor calculation. As the rotation is increased, the flow becomes progressively asymmetric with stabilization/destabilization effects on the cyclonic/anticyclonic sides respectively. These rotation effects, already present in the upstream channel consistently with previous studies, lead further downstream to a reduction/increase of the separation size behind the anticyclonic/cyclonic step. In the cyclonic separation, the free-shear layer created behind the step corner leads to the formation of large-scale spanwise vortices that are found more and more 2D as the rotation is increased. Conversely, in the anticyclonic region, the turbulent structures in the separated layer are more 3D and also more active to promote the reattachment. In the present flow configuration where Coriolis forces do not work while being passive on a purely 2D dynamics, the phenomenological model of absolute vortex stretching is useful to understand how the rotation influences the flow dynamics.

INTRODUCTION

The influence of solid body rotation on turbulent flows can be observed in geophysical or industrial situation. Prediction of rotating flow is an important issue in turbomachinary,
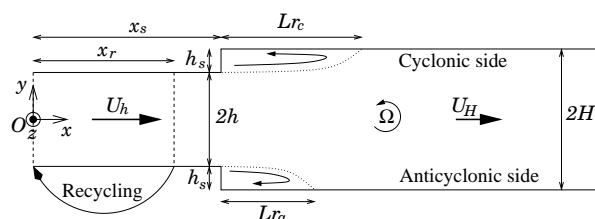

Figure 1.   Schematic view of the flow configuration.

especially for duct flows with separated regions that can modify drastically the efficiency of cooling mechanisms in pumps or turbines. As a generic internal flow, the plane channel configuration has been extensively investigated both experimentally and numerically in turbulent regime, with and without rotation. Conversely, few studies on the effects of a sudden expansion in a plane channel can be found in the literature, especially for numerical results on the turbulent regime, in the rotating [1] as well as in the non-rotating case [2]. The goal of the present study is to investigate by DNS the influence of a spanwise rotation on the dynamics of the two separations due to a sudden symmetric expansion in a turbulent plane channel flow.

FLOW AND NUMERICAL CONFIGURATION

A schematic view of the flow configuration is presented in figure 1. The half-widths of the upstream and downstream channels are h and H respectively with $H > h$, leading to $h_s = H - h$ for the height of each backward facing step. Upstream from the expansion, the flow is assumed to be fully
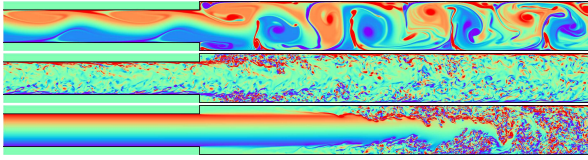
Figure 2. Spanwise vorticity maps. 2D (top) and 3D (middle) DNS with inflow recycling, 3D DNS with laminar inflow conditions (bottom).

Figure 3. Fluctuating velocities (left) and pressure (right) profiles in wall units for the upstream channel $0 < x < x_r$.

developed with a bulk velocity U_h. The rotation vector $\mathbf{\Omega} = (0, 0, \Omega)$ is oriented along the spanwise z-direction. By convention, the rotation rate Ω is assumed positive, so that anticyclonic/cyclonic walls are located in negative/positive values of y. Anticyclonic/cyclonic regions are also frequently referred as pressure/suction or leading/trailing sides respectively, especially in turbomachinary. The present flow configuration can be fully determined by three non-dimensional parameters: the Reynolds number $Re = U_h h / \nu$, the global Rossby number $Ro_g = 3U_h / 2\Omega h$ and the expansion ratio $Er = H/h$. The present definition of Rossby number corresponds to the ratio of the maximum vorticity at the wall $(3U_h/h)$ in a laminar situation (upstream from the expansion) upon the entrainment vorticity (2Ω). Due to the mass conservation, the bulk velocity downstream from the expansion is given by $U_H H = U_h h$ so that the Reynolds number can also be written as $Re = U_H H / \nu$. Conversely, a global Rossby number based on (U_H, H) is given by Ro_g / Er^2 so that the rotation effects are expected to be stronger in the downstream channel. In this study, we investigate a single flow configuration $Re = 5000$ and $Er = 1.5$ by comparing four rotation regimes $Ro_g = \infty, 27, 9, 3$.

The finite difference code "Incompact3d" [3, 4] is used to solve the incompressible Navier-Stokes equations written in the rotating frame of reference by adding the Coriolis term $2\mathbf{\Omega} \times \mathbf{u}$. The computational domain $L_x \times L_y \times L_z = 24H \times 2H \times 6H$ is discretized on a Cartesian grid (slightly stretched in y) of $n_x \times n_y \times n_z = 1441 \times 513 \times 768$ points. Both backward facing steps are modelled using a specific immersed boundary method designed to allow the use of high-order schemes (here compact Δx^6) with an accurate imposition of the no-slip condition at the wall [5]. To control aliasing errors, a sixth-order numerical hyperdissipation is used via the viscous term [6]. The channel is suddenly enlarged at $x_s = 8H$. The remaining downstream part of the computational domain $x_s < x < L_x$ is long enough to observe the separation dynamics but too short to expect the reestablishment of a conventional Poiseuille flow before the outlet.

PRELIMINARY NON-ROTATING SIMULATIONS

The present Reynolds number $Re = 5000$ is supercritical with respect to the prediction of the linear stability theory that provides a critical value $Re_c = 3848$ without rotation. In the rotating case, Re_c can be almost two order of magnitude weaker depending on Ω. In consequence, a very long inflow channel should lead to fully developed turbulent conditions upstream from the expansion, with or without rotation.

To mimic realistic inflow conditions, a precursor calculation could be performed by considering a conventional plane channel while assuming periodicity in the longitudinal direc-
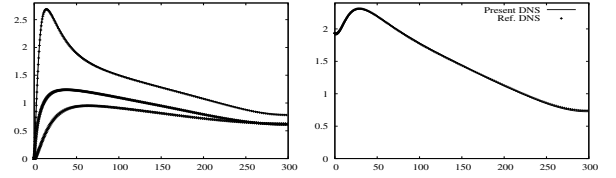
tion. The drawback of this approach is that it requires to synchronize two calculations or to store a substantial amount of instantaneous data to be used as inflow conditions in the main simulation throughout its full duration. To overcome these difficulties, [7] have proposed a method that recycles finite-length time series of a precursor simulation while ensuring a minimal duration of the series actually used. Here, we propose an alternative method by recycling directly the velocity data from a given section $x = x_r$ to the inlet section $x = 0$ at each time step. In the region where the mean flow is parallel, this technique can be performed without any rescaling. In this sense, the calculation generates its own inflow conditions through a process that is purely intrinsic. Expressed mathematically, this definition of inlet conditions seems to lead to a ill-posed problem. However, we have used successfully this very simple technique in 2D and 3D calculations with and without rotation. In addition to its robustness, the method has been found to lead to a very realistic dynamics in the recycled region $0 < x < x_r$, with no significant effect near the inlet despite the use of a simple Dirichlet condition on the velocity at $x = 0$.

Figure 2 (top) presents a vorticity map obtained in a 2D calculation using this recycling technique. The re-use of perturbations introduced only at the initial time is found to allow the development of Tollmien-Schlichting (TS) waves that reach a saturated state with unsteady processes in agreement with the observations of [8]. Here, to allow the amplification of the most unstable TS wave, the recycling length has been adjusted consistently with the linear stability prediction $x_r = 2\pi h$. The ability of present recycling technique to capture the amplification and saturation of TS waves (very sensitive to numerical errors) demonstrates its potential for high accuracy calculations.

Naturally, present 2D TS waves could not be observed in reality because they are very unstable with respect to 3D perturbations. This can be confirmed by performing a 3D calculation where the present recycling is found to lead to a breakdown followed by the establishment of fully developed turbulent conditions. For this 3D DNS, we have used $x_r = 9h$ in order to limit the impact of the longitudinal periodicity introduced by the recycling while feeding the inlet with data not too close from the expansion. The resulting dynamics is illustrated in figure 2 (middle) where a realistic flow dynamics can be observed in the whole channel. As for the 2D calculation, no artefact can be detected near the inlet despite the fully turbulent state recycled here. This point has been confirmed quantitatively through a careful analysis of turbulent statistics (computed using an average in time, x and z) that shows a remarkable homogeneity in the streamwise direction in the recycled region $0 < x < x_r$. An excellent agreement with the ref-
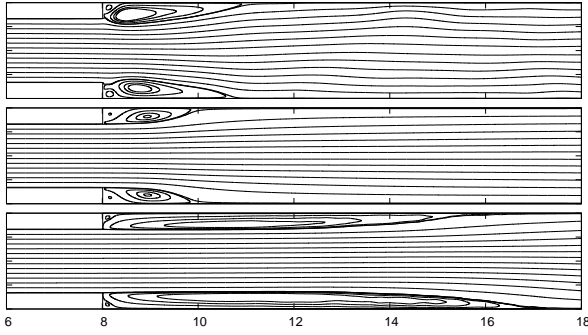
Figure 4.   Mean streamlines. 2D (top) and 3D (middle) DNS with inflow recycling, 3D DNS with laminar inflow conditions (bottom).

erence data of [9] (DNS based on a spectral code) is found for the mean velocity (not shown) as well as for turbulent fluctuations (see figure 3). Note in particular the remarkable agreement of pressure fluctuations that do not seem to be damaged by the recycling. In terms of spatial resolution, present calculation leads to $h^+ \approx 297$, so that DNS requirement is fulfilled in the upstream channel with $\Delta x^+ \approx 7.5$, $1.5 < \Delta y^+ < 3$ and $\Delta z^+ \approx 3.5$. In practice, preliminary calculations have shown that this level of discretization is required to capture correctly the 3D dynamics in the separated regions, these latter being found more demanding in spatial resolution compared with the upstream/downstream channel flows. A last remark concerns the use of immersed boundary method that offers here an accurate prediction of the friction velocity and near-wall turbulent statistics.

An additional 3D DNS has been performed using a laminar Poiseuille velocity profile at the inlet without any recycling procedure. This type of inflow conditions allows the flow to stay laminar up to the expansion. A very long upstream channel should lead to the amplification of TS waves triggered by the numerical noise and followed by a breakdown for a 3D calculation. However, due to the very weak amplification rate of these TS waves, the upstream part of the present computational domain is too short to allow their development. In consequence, this use of a purely laminar inflow condition without recycling leads to two symmetric laminar separations behind the step corners as illustrated in figure 2 (bottom). The reattachment of the flow is then considerably delayed by comparison with the case where the separations are both turbulent using a recycling technique. Quantitatively, the reattachment length Lr (see figure 1 for definition) is found to increase by 300% in the laminar inflow case ($Lr = 24h_s$) by comparison with the inflow turbulent case ($Lr = 6h_s$). These values can be recovered by examining figure 4 where mean streamlines are plotted in each case using an average in time and spanwise direction. For correspondence between H and h_s, note that the geometry imposes $\frac{H}{h_s} = \frac{Er}{Er-1} = 3$. The considerable decrease of Lr when inflow conditions are turbulent is consistent with the natural sensitivity of separated regions with respect to perturbations, fully turbulent conditions being well known to act in favour of reattachment. The reattachment length obtained here is also in good agreement with previous experimental and numerical studies for a backward facing step with turbulent inflow conditions [2, 10] where the reported values are in the range $6h_s < Lr < 7h_s$. Finally, it worth noting that the 2D

calculation leads to the prediction $L_r = 9h_s$, an intermediate value between the laminar and turbulent ones. This calculation, very artificial in first analysis, will be mentioned again in the next section dedicated to comparisons between rotating and non-rotating results.

ROTATING RESULTS

Before the presentation of the rotating results, let us recall some general features of Coriolis forces and rotating channels. In the presence of a spanwise rotation, the symmetry of the channel flow configuration is broken, with one cyclonic side where the vorticity vector is oriented in the same direction as the rotation vector, and one anticyclonic side where these two vectors are in opposite directions. The influence of Coriolis forces has already been investigated previously for a plane channel where stabilizing/destabilizing effects are reported in the cyclonic/anticyclonic regions respectively for a moderate rotation rate. Formally, the present spanwise rotation cannot have any influence on a purely 2D dynamics as the one illustrated in figure 2 (top). In consequence, the influence of Coriolis forces must involve 3D processes. In addition, for a very high rotation rate, the Coriolis forces tend to maintain 2D the flow dynamics, this result being known as the Taylor-Proudman theorem. In this sense, the 2D DNS presented in the previous section provides the expected dynamics for $\Omega \to \infty$ (i.e. $Ro_g \to 0$), as already shown for a conventional plane channel by [11]. Finally, let us mention the phenomenological model of [12] where the destabilizing/stabilizing effects of the rotation are interpreted as the consequence of the promotion/inhibition of the absolute vortex stretching through an increase/reduction of 3D phenomena. In this model, the occurrence of a zero mean absolute vorticity zone (where $\mathbf{W_a} = \mathbf{W} + 2\mathbf{\Omega} \approx \mathbf{0}$) is the most efficient situation to stretch an absolute vortex line and then produce intense streamwise vorticity. These basic mechanisms will be used to interpret the following results.

Rotation effects on the upstream flow

Here, the rotation effects are first examined in the upstream region of the domain $0 < x < x_r$ where a conventional channel flow dynamics is well recovered with or without rotation. The present kinetic energy profiles (figure 5) clearly show the stabilizing effect of the rotation in the cyclonic region where velocity fluctuations are progressively damped as the rotation is increased. The situation is less simple in the anticyclonic side with an increase of the near-wall turbulent kinetic energy at $Ro_g = 27$ but a decrease at $Ro_g = 3$. The stabilizing influence of a cyclonic rotation can be confirmed by the mean velocity profiles (figure 5) with a reduction of the friction velocity and a trend towards laminarization through a shape closer to a laminar Poiseuille flow. Near the anticyclonic wall, the shape of the velocity profiles keeps a turbulent character for the three rotating cases, with an increase of the friction velocity at $Ro_g = 27, 9$ but a decrease at $Ro_g = 3$. An interesting feature of the mean velocity profiles in the rotating cases is the presence of a linear zone in the core of the channel with a shift toward the anticyclonic region. The fundamental reason of this behaviour is not well understood yet. However, an interesting feature is that the slope of this linear part of the
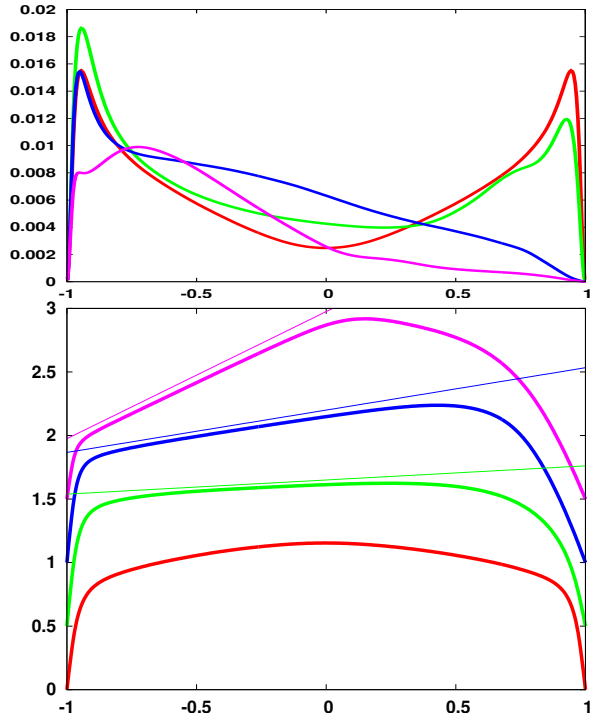
3

Figure 5. Turbulent kinetic energy (top) and mean velocity (bottom) profiles for the upstream channel $0 < x < x_r$. Data in global units (U_h, h) for $Ro_g = \infty$, $Ro_g = 27$, $Ro_g = 9$, $Ro_g = 3$. Thin straightlines in the bottom graph indicate the ideal slope with $dU/dy = 2\Omega$ (zero absolute mean vorticity).

Figure 6. Instantaneous visualization of Q criterion for $Ro_g = \infty, 27, 9, 3$ for $0 < x < x_r$ (from top to bottom).

Figure 7. Spanwise vorticity maps for $Ro_g = \infty, 27, 9, 3$ (from top to bottom).

velocity profiles is directly controlled by the rotation rate and corresponds to the selection of a zero mean absolute vorticity where $-dU/dy + 2\Omega \approx 0$, or equivalently where the local Rossby number (defined as the ratio of the mean vorticity over 2Ω) is given by $Ro(y) \approx -1$. As recalled in the introduction of this section, this zero mean vorticity region is expected to increase the efficiency of absolute vortex stretching and then promote the production of strong streamwise vortices.

This increase of streamwise vorticity by rotation can be observed on fluctuating vorticity profiles (not shown). To have a more accurate view of the dynamics associated with this mechanism, instantaneous visualizations of the Q criterion are presented in figure 6. In addition to the damping of vortical structures by the rotation in the cyclonic side, a clear change of vortex topology can be observed in the anticyclonic region. For the highest rotation rate considered ($Ro_g = 3$), no vortex can be detected in the cyclonic side whereas in the anticyclonic side, the vortices seem to be more organized and also more oriented in the streamwise direction. This trend can be interpreted as the consequence of an increase of the absolute vortex stretching [13], especially in this particular region where the mean absolute vorticity is almost zero, leading to highly 3D absolute vortex lines very easy to stretch by the local shear flow. This important change of the vortex topology before the expansion will be used in the next section to understand how the rotation acts on the separations.
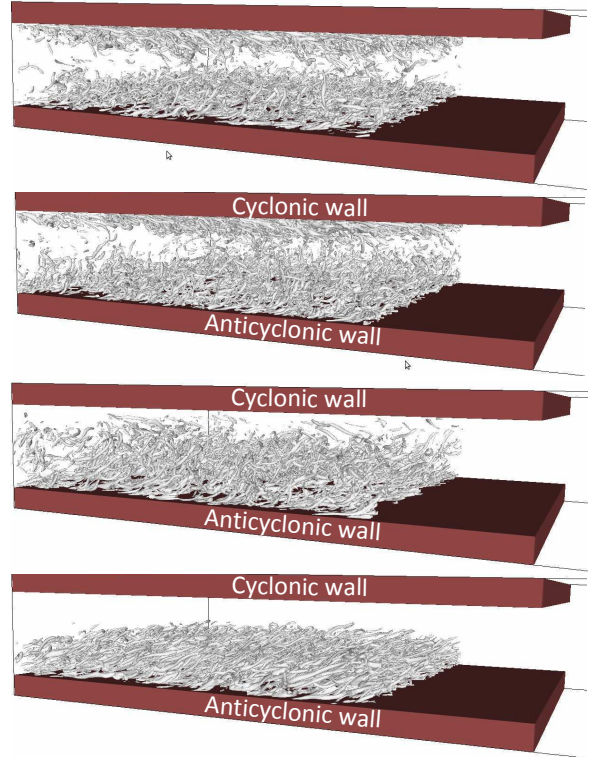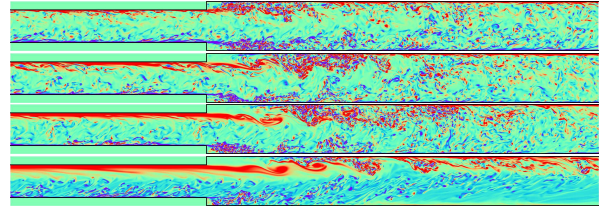
Rotation effects on the mean separations

The 2D maps of spanwise vorticity presented in figure 7 give a first view about the rotation influence on the flow dynamics across the expansion. Basically, the stabilizing/destabilizing rotation effects are recovered in the whole channel, downstream as well as upstream from the expansion. In the cyclonic separation, the free-shear layer behind the step corner leads to the formation of large-scale Kelvin-Helmholtz type vortices. In the non-rotating case, present 2D maps do not allow the clear identification of this type of large-scale structures, as well as in the anticyclonic separation for the rotating cases.

To get a more quantitative information, the mean streamlines across the expansion are compared in figure 8 for the four cases under study. The more remarkable feature is the considerable enlargement of the cyclonic recirculation bubble in the rotating cases. In first analysis, this trend can be associated with the reduction of the turbulent fluctuations in the upstream cyclonic side of the channel by the rotation. Just af-
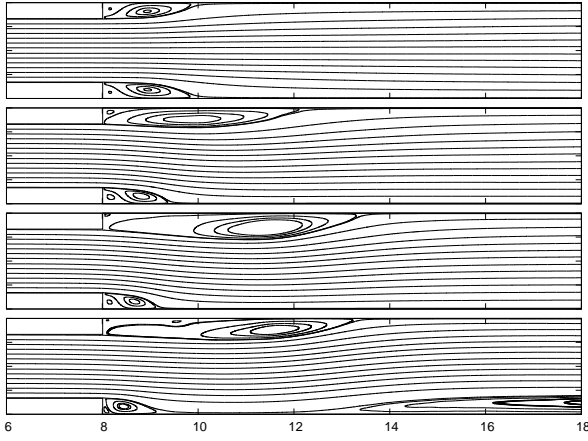
4

Figure 8. Mean streamlines for $Ro_g = \infty, 27, 9, 3$ (from top to bottom).
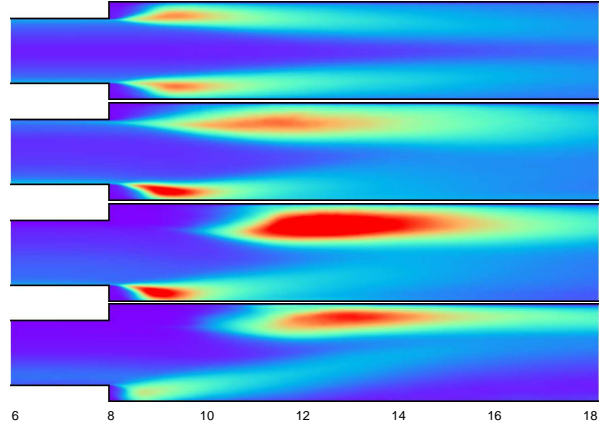

Figure 9. Maps of turbulent kinetic energy k for $Ro_g = \infty, 27, 9, 3$ (from top to bottom). Colour map saturated in red for $k > 0.03 U_h^2$.

ter the expansion, the resulting separated cyclonic shear layer is less perturbed so that it reattaches further downstream by comparison with the non-rotating case. Note that the 175% increase of Lr_c at $Ro_g = 3$ can be related to the 300% increase observed in the previous section when purely laminar inflow conditions are used in a non-rotating channel. Concerning the anticyclonic bubble, the reattachment length is found to decrease as the rotation is increased. This behaviour cannot be simply connected to the turbulent kinetic energy k upstream from the expansion because k is increased at $Ro_g = 27$ but reduced at $Ro_g = 3$ (see figure 5) whereas the bubble size is reduced in both cases. An interpretation of the reduction of Lr_a at $Ro_g = 3$ despite the lowest level of near-wall turbulent fluctuations will be proposed in the next subsections through an investigation of the vortical structures. Note that present reduction/increase of Lr_a/Lr_c is consistent with the observations of [1, 14] and the recent measurements of [15].

An unexpected phenomenon is the formation further downstream of a second recirculation bubble near the anticyclonic wall at $Ro_g = 3$. We interpret this secondary separation as the consequence of the adverse pressure gradient due to the reattachment in the cyclonic region. Actually, the enlargement of the cyclonic bubble imposes an acceleration of the flow followed by a deceleration when the bubble starts to close up. Combined with the reduction of the anticyclonic friction velocity due to the rotation, the resulting adverse pressure gradient leads the anticyclonic flow to separate at almost the same streamwise location as the cyclonic reattachment. Note that the formation of this second recirculation bubble at $Ro_g = 3$ can be seen as marginal because this phenomenon is not observed at $Ro_g = 9$ despite a similar adverse pressure gradient. In the latter case, the stronger anticyclonic turbulent fluctuations and friction velocity are enough to prevent the flow to separate despite the deceleration.

To have an overview of the turbulence level in the whole channel, maps of turbulent kinetic energy are presented in figure 9. The downstream shift of the reattachment in the cyclonic region leads to an increase of k around the reattachment (despite the reduction of k at the separation start), but this increase is less marked at $Ro_g = 3$. For the anticyclonic separation, an increase of k can be observed at $Ro_g = 27$ against a decrease for $Ro_g = 3$, consistently with the rotation effects in

the upstream channel.

Rotation effects on the separation vortices

To give an insight into the physical mechanisms driving the rotation influence on the size of cyclonic/anticyclonic separation bubbles, instantaneous visualizations of the Q criterion in the expansion region are presented in figure 10. For clarity, only one side of the channel is exhibited for each visualization by focusing on the non- and high-rotating cases ($Ro_g = \infty, 3$). In the non-rotating case, using the present Q criterion visualizations (that emphasize fine scale turbulence), no large scale structure extending along the full span of the separation bubble can be clearly identified. On the contrary, in the rotating case, as already suggested by the maps of spanwise vorticity (figure 7), we observe the formation of large scale vortices in the cyclonic separation. These structures are more and more 2D as the rotation is increased. For the highest rotation rate ($Ro_g = 3$), they are quasi-2D as shown in figure 10. This rotation effect can be interpreted as the consequence of the inhibition of the absolute vortex stretching by the locally cyclonic rotation.

In the anticyclonic side, as in the upstream channel, the rotation is found to promote the production of longitudinal vortices that can be observed at the top of the separation, especially for the highest rotation rate presented in figure 10. These longitudinal vortices are probably the key reason of the reduction of Lr_a. In first analysis, the reduction of turbulent fluctuations in the anticyclonic bubble should lead to an increase of Lr_a. However, the exact vortex topology can also play a role in the physical processes that help more or less efficiently the flow to reattach. Our interpretation is that the strong longitudinal vortices developing at the top of the anticyclonic separation are very efficient to increase the momentum exchange across the separated layer and then promote the reattachment despite the moderate level of turbulence. In the non-rotating separations, the vortical structures are more energetic but less organized, reducing the efficiency of the momentum transfer and the ability of the flow to reattach. This fundamental difference can be directly observed in figure 11 through a streamwise vorticity cut located just be-
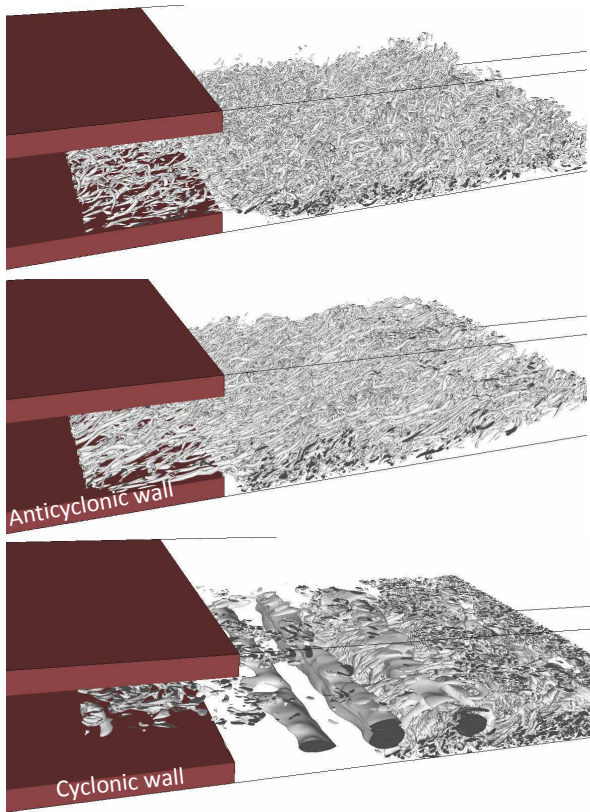
Figure 10. Instantaneous visualization of Q criterion for $Ro_g = \infty$ (top) and $Ro_g = 3$ (middle and bottom).
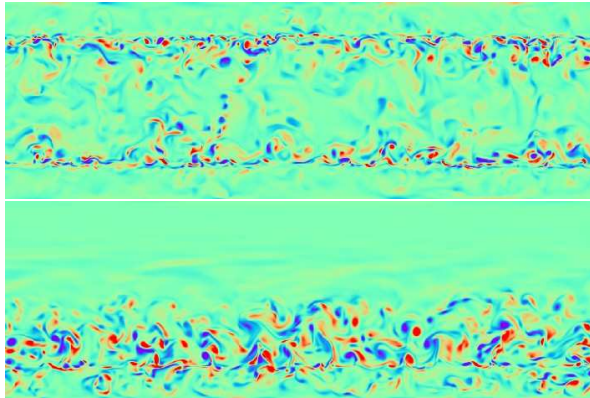

Figure 11. Maps of streamwise vorticity at $x = 8.13H$ for $Ro_g = \infty$ (top) and $Ro_g = 3$ (bottom).

hind the steps at $x = 8.13H$ for $Ro_g = \infty, 3$. The numerous, strong and regularly spaced longitudinal vortices observed at $Ro_g = 3$ are in contrast with the ones of the non-rotating case, suggesting again the reinforcement of mechanisms promoting the reattachment despite the weaker level of near-wall turbulence upstream from the separation.

CONCLUSION

The present study is the first investigation by DNS of the influence of a spanwise rotation on the two separations due to a sudden symmetric expansion inside a channel flow. The physical mechanisms of the modifications introduced by the Coriolis forces on the flow are exhibited and interpreted in terms of vortex dynamics governed by the absolute vorticity equation. An interesting property of present calculations is that they use a convenient recycling method to provide a realistic turbulent state at the inlet, in the rotating as well as in the non-rotating cases. Statistically, all the boundary conditions are unambiguously defined. In consequence, the present flow configuration could be an interesting benchmark useful to develop more accurate turbulence modelling in the context of RANS or hybrid RANS-LES of internal rotating flows.

REFERENCES

[1] M. Barri and H. I. Andersson, *J. Fluid Mech.*, vol. 665, pp. 382–417, 2010.

[2] M. Barri, G. K. E. Khoury, H. I. Andersson, and B. Pettersen, *Int. J. Numer. Methods Fluids*, vol. 64, pp. 777–792, 2009.

[3] S. Laizet and E. Lamballais, *J. Comp. Phys.*, vol. 228, pp. 5989–6015, 2009.

[4] S. Laizet, E. Lamballais, and J. C. Vassilicos, *Computers and Fluids*, vol. 39, no. 3, pp. 471–484, 2010.

[5] P. Parnaudeau, J. Carlier, D. Heitz, and E. Lamballais, *Phys. Fluids*, vol. 20, no. 085101, 2008.

[6] E. Lamballais, V. Fortuné, and S. Laizet, *J. Comp. Phys.*, vol. 230, pp. 3270–3275, 2011.

[7] M. Barri, G. K. E. Khoury, H. I. Andersson, and B. Pettersen, *Int. J. Numer. Methods Fluids*, vol. 60, pp. 227–235, 2009.

[8] J. Jiménez, *J. Fluid Mech.*, vol. 218, pp. 265–297, 1990.

[9] K. Iwamoto, Y. Suzuki, and N. Kasagi, *Int. J. Heat and Fluid Flow*, vol. 23, no. 5, pp. 678–689, 2002.

[10] H. Le, P. Moin, and J. Kim, *J. Fluid Mech.*, vol. 330, pp. 349–374, 1997.

[11] E. Lamballais, M. Lesieur, and O. Métais, and turbulent channel flow," *Int. J. Heat and Fluid Flow*, vol. 17, no. 3, pp. 324–332, 1996.

[12] M. Lesieur, S. Yanase, and O. Métais, *Phys. Fluids A*, vol. 3, pp. 403–407, 1991.

[13] E. Lamballais, O. Métais, and M. Lesieur, *Theoret. Comput. Fluid Dynamics*, vol. 12, 1998.

[14] P. H. Rothe and I. P. Johnston, *Journal of Fluids Engineering. Trans. ASME*, vol. 101, pp. 117–120, 1979.

[15] J. Visscher and H. I. Andersson, in *Proc. of the Hydralab III Joint User Meeting*, (Hannover), 2010.